# Propagation properties of electromagnetic fields in elliptic dielectric hollow fibres and their applications*

Li Hui-Rong(李会容) and Yin Jian-Ping(印建平)†

*State Key Laboratory of Precision Spectroscopy, Department of Physics, East China Normal University, Shanghai* 200062, *China*

(Received 9 December 2009; revised manuscript received 6 January 2010)

We numerically calculate and analyse the electromagnetic fields, optical intensity distributions, polarization states and orbital angular momentum of some elliptic hollow modes in an elliptic dielectric hollow fiber (EDHF) by using Mathieu functions, and also calculate the optical potential of the blue-detuned $_{e}HE_{11}$ mode evanescent-light wave for $^{85}$Rb atoms, including the position-dependent van der Waals potential, and discuss briefly some potential applications of our EDHF in atom and molecule optics, etc. Our study shows that the vector electric field distributions of the odd modes in the cross section of the EDHF are the same as that of the even modes and with different boundary ellipses by rotating an angle of $\pi/2$, and the orbital angular momentum (OAM) of single HE (EH) mode is exactly equal to zero, while that of dual-mode in the EDHF is fractional in $\hbar$, and has a sinusoidal oscillation as $z$ varies. The EDHF can be used to produce various elliptic hollow beams, even to generate and study various atomic vortices with a fractional charge and its fractional quantum Hall effect in atomic Bose–Einstein condensate, and so on.

**Keywords:** elliptic hollow modes, optical potential, orbital angular momentum, polarisation

**PACC:** 3280P, 4110, 4281D, 4225J

## 1. Introduction

Optical fibres have wide applications in the fields of radar feed line, optical communication, fibre lasers, microwave heating applicator, electron accelerator, and so on.[1,2] Recently, varieties of applications with the hollow fibres have been proposed and experimentally demonstrated, such as a mode converter for high-order mode dispersion compensation,[3] generation of dark hollow beam,[4,5] laser guiding of cold atoms[6−9] and an atomic funnel,[10,11] etc. It is well known that when compared with a circular cylinder fibre, the attenuation of the dominant mode in an elliptic fibre with the same cross-section area will be reduced and the transmission modes in the elliptic fibre will be stable.[12,13] Therefore, an elliptic hollow fibre is superior to a circular hollow one in some aspects, and has wider applications.

In 1938, Chu[13] first analysed theoretically the transmission of the electromagnetic waves in elliptic metallic hollow pipes, and gave the cutoff frequencies and field configurations of six wave modes. From then on, the elliptical waveguide was investigated both theoretically and experimentally. In the 1970s, Kretzschmar pointed out Chu's wrong analysis for the $TM_{c01}$ mode fields and modified the corresponding configuration presented by Chu.[14,15] Since Chu's expansion of Mathieu functions was only valid for large $\xi$, Falciasecca *et al.*[16−18] studied and generalized it. The impedance of an elliptical waveguide was early calculated in 1960.[19] In 1962, Yeh[12] derived the eigenfunctions and the characteristic roots of the two dominant modes in the elliptical dielectric waveguide. Using Yeh's eigenfunctions, Rengarajan *et al.* investigated the propagation characteristics of the modes in the elliptical metallic waveguide filled with a dielectric layer.[2] Subsequently, they investigated theoretically the single mode propagation in three-layer step index elliptical fibre waveguides.[20] Furthermore, several methods for calculating the eigenmode sequence and cutoff wavelength of the elliptic hollow waveguide were presented in the last two decades,[21−24] and the propagation characteristics of confocal elliptical waveguide loaded with multi-layered dielectrics were discussed.[25] In 2007, Halterman *et al.* investigated the propagation characteristics and the local energy-density in the open elliptical metallic waveguide.[26] Gómez-Castellanos[27] reported the intensity distributions and cutoff frequencies of linearly polarized modes

*Project supported by the National Natural Science Foundation of China (Grant Nos. 10374029, 10434060 and 10674047), the National Key Basic Research and Development Program of China (Grant No. 2006CB921604), the Basic Key Program of Shanghai Municipality (Grant No. 07JC14017), the Program for Changjiang Scholar and Innovative Research Team, and Shanghai Leading Academic Discipline Project (Grant No. B408).

†Corresponding author. E-mail: jpyin@phy.ecnu.edu.cn

© 2010 Chinese Physical Society and IOP Publishing Ltd

for a step-index elliptical optical fibre. More recently, a novel super-Gaussian approximation method was proposed to calculate the propagation and dispersion characteristics of the elliptical core fibre.[28]

In this paper, we study some other propagation properties of the electromagnetic field in a micron-sized elliptic dielectric hollow fibre (EDHF) composed of three confocal and concentric elliptical layers and discuss its potential applications. In Secion 2, using Mathieu functions, we numerically calculate and analyse the electromagnetic field and optical intensity distributions, the polarisation states and orbital angular momentum of some elliptic hollow modes in the EDHF, and briefly analyse a dual-mode transmission in the EDHF. In Section 3, we calculate the optical potential of the ${}_{\rm e}{\rm HE}_{11}$ modes for cold ${}^{85}$Rb atoms, including the position-dependent van der Waals attractive potential from the inner wall of the hollow core, and discuss some potential applications of these special modes. In the last section, we summarize the main results and conclusions.

## 2. Numerical calculation and analysis

### 2.1. The magnetic and electric field distributions in EDHF

A hollow optical fibre with an elliptical cross section and its orthogonal elliptic coordinate system ($\xi$, $\eta$, $z$) are shown in Figs. 1(a) and 1(b), respectively. Usually, the orthogonal elliptic coordinates ($\xi$, $\eta$, $z$) are used to solve Maxwell's equations with elliptic boundaries, and defined in terms of a right-hand Cartesian system by the following equations

$$x = h\cosh\xi\cos\eta, \quad y = h\sinh\xi\sin\eta, \quad z = z, \quad (1)$$

where $\xi$ and $\eta$ takes the value $0 \leq \xi < +\infty$, $0 \leq \eta < 2\pi$, respectively; $h$ represents half way of the distance between the foci $F$ and $F'$. The $z$ axis is set to accord with the longitudinal axis of the EDHF. The EDHF consists of three layers: a hollow region, a core and a cladding, and the cylindrically symmetric refractive indices of them are $n_0$, $n_1$ and $n_2$, respectively. In Fig. 1(b), the contour surfaces of the constant $\xi$ are confocal and concentric elliptical cylinders, while those of the constant $\eta$ are confocal hyperbolic cylinders orthogonal to the elliptical cylinders. The inner boundary of the core is located at $\xi = \xi_0$, and its eccentricity $e$ is given by $1/\cosh\xi_0$, while the semi-major axis and the semi-minor axis of the boundary ellipse are $a = h\cosh\xi_0$ and $b = h\sinh\xi_0$, respectively. And $\xi_1$ and $\xi_2$ are the outer boundary of the hollow core and the cladding.

We assume the parameters of the EDHF to be: $n_0 = 1$, $n_1 = 1.4530$, $n_2 = 1.4502$, $e = 0.46$, $\xi_0 = 1.40$, $\xi_1 = 2.34$, and $\xi_2$ is taken to be infinity. The incident laser wavelength is $\lambda = 0.78$ $\mu$m. The electromagnetic fields in the EDHF are supposed to vary harmonically in time and propagate in the positive $z$ direction, which will result in a multiplication of all wave functions by $\exp[{\rm i}(\omega t - \beta z)]$. In the EDHF investigated here, all modes should be the hybrid ones (i.e. $E_z$ and $H_z$ both exist).[12]

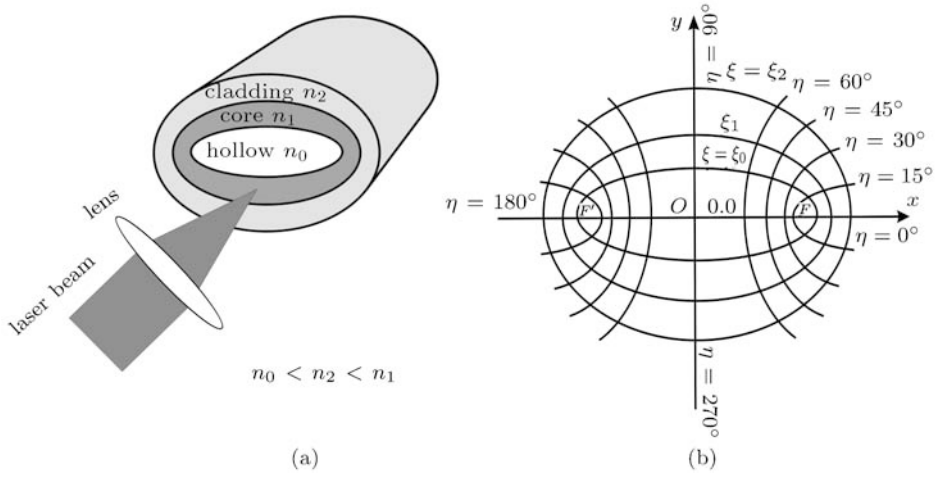



**Fig. 1.** (a) Structure of EDHF and excitation scheme. (b) The corresponding orthogonal elliptic coordinate system. EDHF is composed of a hollow region, a core and a cladding, and their refractive indices are $n_0$, $n_1$ and $n_2$, respectively.

We use ${}_{\rm e}{\rm HE}_{mn}$ and ${}_{\rm o}{\rm HE}_{mn}$ (${}_{\rm e}{\rm EH}_{mn}$ and ${}_{\rm o}{\rm EH}_{mn}$) to denote the mode types in the EDHF. The first prescript e and o represent respectively even and odd modes, while the first subscript $m$ represents the order of the Mathieu functions or the modified Mathieu functions, and the second subscript $n$ is the order of the parametric zero of the eigenvalue equation of a certain mode. We assume that the incident light is coupled into the core region of the EDHF as shown in Fig. 1(a). Some hybrid modes will be excited selectively, and there will be evanescent-light waves near the elliptic inner boundary of the core. From Maxwell's equations we obtain the following Helmholtz wave equation for the longitudinal component $E_z$ or $H_z$ in the orthogonal elliptical coordinate system:

$$\left[\frac{\partial^2}{\partial\xi^2}+\frac{\partial^2}{\partial\eta^2}+2q(\cosh 2\xi-\cos 2\eta)\right]\begin{bmatrix}E_z\\H_z\end{bmatrix}=0, \quad (2)$$

where

$$q\equiv\frac{k^2-\beta^2}{4}h^2, \quad k=nk_0, \quad h=ae, \quad (3)$$

and $k_0$ is the wave number in the vacuum. Using the method of separation of variables, we obtain the following solution for the wave equation

$$\psi(\xi,\eta,z)=\begin{bmatrix}(A_m{\rm Je}_m(\xi,q)+B_m{\rm Ye}_m(\xi,q)){\rm Se}_m(\eta,q)\\(C_m{\rm Jo}_m(\xi,q)+D_m{\rm Yo}_m(\xi,q)){\rm So}_m(\eta,q)\end{bmatrix}\exp[{\rm i}(\omega t-\beta z)]. \quad (4)$$

For simplicity, the factor $\exp[{\rm i}(\omega t-\beta z)]$ in the following formulae is omitted. ${\rm Se}_m(\eta,\, q_i)$ and ${\rm So}_m(\eta,\, q_i)$ denote the circumferential first-kind even and odd Mathieu functions; ${\rm Je}_m(\xi,\, q_i)$ and ${\rm Jo}_m(\xi,\, q_i)$, and ${\rm Ye}_m(\xi,\, q_i)$ and ${\rm Yo}_m(\xi,\, q_i)$ denote the radial first-kind and second-kind even and odd Mathieu functions of order $m$ ($m=0,\,1,\,2,\,\ldots,\,N$), respectively. And the radial Mathieu functions will be the corresponding Bessel functions ${\rm J}_m$ and ${\rm Y}_m$ when $q_i\to 0$. In the case of $q_i<0$, the circumferential and radial Mathieu functions ${\rm Se}_m(\eta,\, q_i)$ and ${\rm So}_m(\eta,\, q_i)$, ${\rm Je}_m(\xi,\, q_i)$ and ${\rm Jo}_m(\xi,\, q_i)$, ${\rm Ye}_m(\xi,\, q_i)$ and ${\rm Yo}_m(\xi,\, q_i)$ should be the relevant modified Mathieu functions ${\rm Qe}_m(\eta,\,-q_i)$ and ${\rm Qo}_m(\eta,\,-q_i)$, ${\rm Ie}_m(\xi,\,-q_i)$ and ${\rm Io}_m(\xi,\,-q_i)$, ${\rm Ke}_m(\xi,\,-q_i)$ and ${\rm Ko}_m(\xi,\,-q_i)$.[28] The longitudinal magnetic fields of an even (odd) mode are represented by even (odd) Mathieu functions, and the longitudinal electric fields of an even (odd) mode are in terms of odd (even) Mathieu functions.[12]

We take the ${}_{\rm e}{\rm HE}_{11}$ mode as an example. And using the first order of modified and ordinary Mathieu functions,[29–31] we can write the magnetic and electric fields propagating along the $z$-axis in the EDHF

$$H_z=\begin{cases}A{\rm Ie}_1(\xi,q_1){\rm Qe}_1(\eta,q_1), & 0\le\xi\le\xi_0,\\ [B{\rm Je}_1(\xi,q_2)+C{\rm Ye}_1(\xi,q_2)]{\rm Se}_1(\eta,q_2), & \xi_0<\xi\le\xi_1,\\ D{\rm Ke}_1(\xi,q_3){\rm Qe}_1(\eta,q_3), & \xi_1<\xi<\infty;\end{cases} \quad (5)$$

$$E_z=\begin{cases}A'{\rm Io}_1(\xi,q_1){\rm Qo}_1(\eta,q_1), & 0\le\xi\le\xi_0,\\ [B'{\rm Jo}_1(\xi,q_2)+C'{\rm Yo}_1(\xi,q_2)]{\rm So}_1(\eta,q_2), & \xi_0<\xi\le\xi_1,\\ D'{\rm Ko}_1(\xi,q_3){\rm Qo}_1(\eta,q_3), & \xi_1<\xi<\infty;\end{cases} \quad (6)$$

Here $A$, $B$, $C$, $D$, $A'$, $B'$, $C'$, and $D'$ are the eight constants dependent on the boundary conditions. Using Maxwell's equations once again, we can obtain the relations between the transverse and the longitudinal electromagnetic field components

$$\begin{cases}E_{\eta i}=\dfrac{-{\rm i}}{h_i\sqrt{\sinh^2\xi+\sin^2\eta}(k_0^2n_i^2-\beta^2)}\left[\beta\dfrac{\partial E_{zi}}{\partial\eta}-\omega\mu\dfrac{\partial H_{zi}}{\partial\xi}\right],\\ H_{\eta i}=\dfrac{-{\rm i}}{h_i\sqrt{\sinh^2\xi+\sin^2\eta}(k_0^2n_i^2-\beta^2)}\left[\omega\varepsilon_i\dfrac{\partial E_{zi}}{\partial\xi}+\beta\dfrac{\partial H_{zi}}{\partial\eta}\right],\\ E_{\xi i}=\dfrac{-{\rm i}}{h_i\sqrt{\sinh^2\xi+\sin^2\eta}(k_0^2n_i^2-\beta^2)}\left[\beta\dfrac{\partial E_{zi}}{\partial\xi}+\omega\mu\dfrac{\partial H_{zi}}{\partial\eta}\right],\\ H_{\xi i}=\dfrac{-{\rm i}}{h_i\sqrt{\sinh^2\xi+\sin^2\eta}(k_0^2n_i^2-\beta^2)}\left[-\omega\varepsilon_i\dfrac{\partial E_{zi}}{\partial\eta}+\beta\dfrac{\partial H_{zi}}{\partial\xi}\right],\end{cases} \quad (7)$$

where $\omega$ is the angular frequency of the laser light, $\beta$ is the axial propagation constant, and the other parameters are defined as, respectively

$$q_1 = h_1^2(\beta^2 - k_0^2 n_0^2)/4, \quad q_2 = h_2^2(k_0^2 n_1^2 - \beta^2)/4, \quad q_3 = h_3^2(\beta^2 - k_0^2 n_2^2)/4, \quad h_i = \sqrt{a_i^2 - b_i^2}, \quad i = 1, 2, 3. \tag{8}$$

From Eqs. (5)–(7), we obtain the transverse component of electric and magnetic fields of the ${}_{\rm e}{\rm HE}_{11}$ mode. Since $H_z$, $E_z$, $H_\eta$, and $E_\eta$ are continuous at $\xi = \xi_0$ and $\xi = \xi_1$, we have the eigenvalue equation

$$\begin{pmatrix}
\chi_1 {\rm Ie}_1(\xi_0, q_1) & -\chi_2 {\rm Je}_1(\xi_0, q_2) & -\chi_2 {\rm Ye}_1(\xi_0, q_2) & 0 & 0 & 0 & 0 & 0 \\
0 & \chi_2 {\rm Je}_1(\xi_1, q_2) & \chi_2 {\rm Ye}_1(\xi_1, q_2) & -\chi_3 {\rm Ke}_1(\xi_1, q_3) & 0 & 0 & 0 & 0 \\
0 & 0 & 0 & 0 & \chi_4 {\rm Io}_1(\xi_0, q_1) & -\chi_5 {\rm Jo}_1(\xi_0, q_2) & -\chi_5 {\rm Yo}_1(\xi_0, q_2) & 0 \\
0 & 0 & 0 & 0 & 0 & \chi_5 {\rm Jo}_1(\xi_1, q_2) & \chi_5 {\rm Yo}_1(\xi_1, q_2) & -\chi_6 {\rm Ko}_1(\xi_1, q_3) \\
-\omega\mu\alpha_1\chi_1 {\rm Ie}_1'(\xi_0, q_1) & \omega\mu\chi_2 {\rm Je}_1'(\xi_0, q_2) & \omega\mu\chi_2 {\rm Ye}_1'(\xi_0, q_2) & 0 & \beta\alpha_1\chi_7 {\rm Io}_1(\xi_0, q_1) & -\beta\chi_8 {\rm Jo}_1(\xi_0, q_2) & -\beta\chi_8 {\rm Yo}_1(\xi_0, q_2) & 0 \\
0 & -\omega\mu\alpha_2\chi_2 {\rm Je}_1'(\xi_1, q_2) & -\omega\mu\alpha_2\chi_2 {\rm Ye}_1'(\xi_1, q_2) & \omega\mu\chi_3 {\rm Ke}_1'(\xi_1, q_3) & 0 & \beta\chi_8 {\rm Jo}_1(\xi_1, q_2) & \beta\chi_8 {\rm Yo}_1(\xi_1, q_2) & -\beta\chi_9 {\rm Ko}_1(\xi_1, q_3) \\
\beta\alpha_1\chi_{10} {\rm Ie}_1(\xi_0, q_1) & -\beta\chi_{11} {\rm Je}_1(\xi_0, q_2) & -\beta\chi_{11} {\rm Ye}_1(\xi_0, q_2) & 0 & \omega\varepsilon_0 n_0^2 \alpha_1 \chi_4 {\rm Io}_1'(\xi_0, q_1) & -\omega\varepsilon_0 n_1^2 \chi_5 {\rm Jo}_1'(\xi_0, q_2) & -\omega\varepsilon_0 n_1^2 \chi_5 {\rm Yo}_1'(\xi_0, q_2) & 0 \\
0 & \beta\alpha_2\chi_{11} {\rm Je}_1'(\xi_1, q_2) & \beta\alpha_2\chi_{11} {\rm Ye}_1'(\xi_1, q_2) & -\chi_{12} {\rm Ke}_1(\xi_1, q_3) & 0 & \omega\varepsilon_0 n_1^2 \alpha_2 \chi_5 {\rm Jo}_1'(\xi_1, q_2) & \omega\varepsilon_0 n_1^2 \alpha_2 \chi_5 {\rm Yo}_1'(\xi_1, q_2) & -\omega\varepsilon_0 n_2^2 \chi_6 {\rm Ko}_1'(\xi_1, q_3)
\end{pmatrix}
\begin{pmatrix} A \\ B \\ C \\ D \\ A' \\ B' \\ C' \\ D' \end{pmatrix} = 0. \tag{9}$$

Here $h_1 = h_2 = h_3$, and

$$\begin{aligned}
&\alpha_i = (k_0^2 n_{i+1}^2 - \beta^2)/(k_0^2 n_i^2 - \beta^2), \quad i = 0, 1, \\
&\chi_1 = \int_0^{2\pi} {\rm Qe}_1(\eta, q_1){\rm Se}_1(\eta, q_2){\rm d}\eta, \\
&\chi_2 = \int_0^{2\pi} {\rm Se}_1^2(\eta, q_2){\rm d}\eta, \\
&\chi_3 = \int_0^{2\pi} {\rm Qe}_1(\eta, q_3){\rm Se}_1(\eta, q_2){\rm d}\eta, \\
&\chi_4 = \int_0^{2\pi} {\rm Qo}_1(\eta, q_1){\rm So}_1(\eta, q_2){\rm d}\eta, \\
&\chi_5 = \int_0^{2\pi} {\rm So}_1^2(\eta, q_2){\rm d}\eta, \\
&\chi_6 = \int_0^{2\pi} {\rm Qo}_1(\eta, q_3){\rm So}_1(\eta, q_2){\rm d}\eta, \\
&\chi_7 = \int_0^{2\pi} {\rm Qo}_1'(\eta, q_1){\rm Se}_1(\eta, q_2){\rm d}\eta, \\
&\chi_8 = \int_0^{2\pi} {\rm So}_1'(\eta, q_2){\rm Se}_1(\eta, q_2){\rm d}\eta, \\
&\chi_9 = \int_0^{2\pi} {\rm Qo}_1'(\eta, q_3){\rm Se}_1(\eta, q_2){\rm d}\eta, \\
&\chi_{10} = \int_0^{2\pi} {\rm Qe}_1'(\eta, q_1){\rm So}_1(\eta, q_2){\rm d}\eta, \\
&\chi_{11} = \int_0^{2\pi} {\rm Se}_1'(\eta, q_2){\rm So}_1(\eta, q_2){\rm d}\eta, \\
&\chi_{12} = \int_0^{2\pi} {\rm Qe}_1'(\eta, q_3){\rm So}_1(\eta, q_2){\rm d}\eta.
\end{aligned} \tag{10}$$

In order to obtain a set of nontrivial solutions of $A$, $B$, $C$, $D$, $A'$, $B'$, $C'$, and $D'$, we set the determinant of the parameters matrix in Eqs. (9) to zero, and a transcendental equation is obtained for seeking the propagation constant $\beta$. The propagation constant $\beta_1$ of the ${}_{\rm e}{\rm HE}_{11}$ mode equals the first characteristic root of this eigenvalue equation. Then we substitute $\beta_1$ into the boundary conditions Eqs. (9) so as to obtain the relations between $A$, $B$, $C$, $D$, $A'$, $B'$, $C'$, and $D'$, and find the electric and magnetic field distributions of the ${}_{\rm e}{\rm HE}_{11}$ mode by Eqs. (7). We can deal with the other modes in the same manner. The eigenvalue equation of the even mode is obtained by changing the order of the Mathieu functions and modified Mathieu functions. As to the odd mode, it still needs to exchange $\varepsilon_0 n_i^2$ and $-\mu$.

Figure 2 indicates all electromagnetic field components of the ${}_{\rm e}{\rm HE}_{11}$ mode as functions $\xi$ for five dif-

ferent values of the angular coordinate $\eta$. It is clear that the electromagnetic field component distributions for five different $\eta$ have a similar profiles; however, $H_z$, $H_\xi$, $H_\eta$, $E_z$, and $E_\eta$ experience continuous evolutions, while $E_\xi$ suffers a discontinuous transition, which are consistent with the boundary conditions. Also, it obviously shows that the electromagnetic fields are concentrated in the core region, and they flow outward and gradually vanish near the inner and the outer boundaries ($\xi_0$ and $\xi_1$) of the core. Those electromagnetic field distributions of the ${}_{\rm e}{\rm HE}_{13}$ mode and the ${}_{\rm e}{\rm HE}_{15}$ one in Figs. 3 and 4 have the same behaviour.

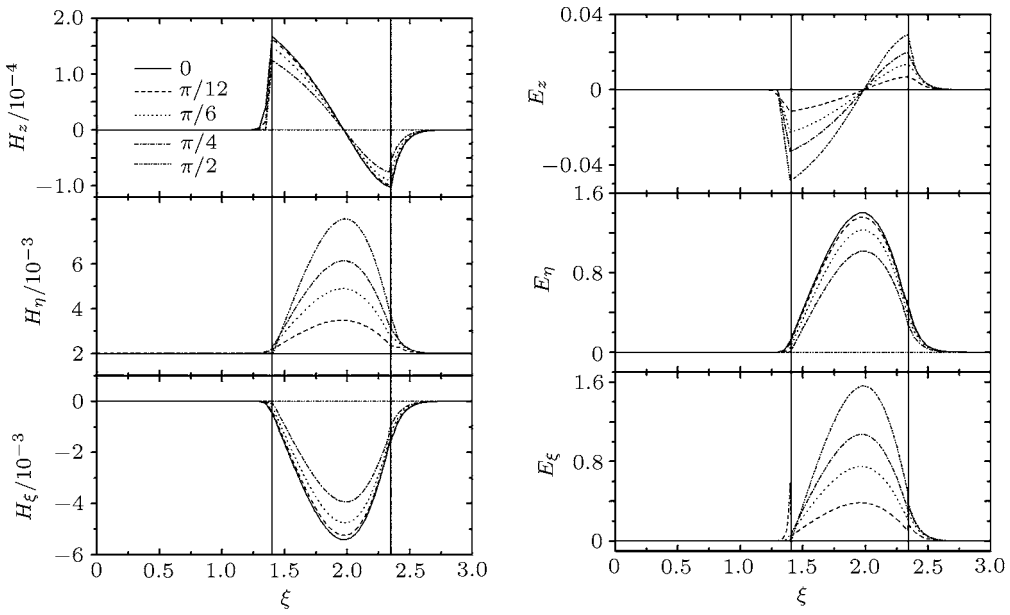



**Fig. 2.** The distributions of electric and magnetic fields for the ${}_{\rm e}{\rm HE}_{11}$ mode in the EDHF as functions of the radial position $\xi$. The parameters of the EDHF are $n_0 = 1$, $n_1 = 1.4530$, $n_2 = 1.4502$, $e = 0.46$, $\xi_0 = 1.40$, $\xi_1 = 2.34$. Here $\xi_0$ and $\xi_1$ are respectively the inner and the outer boundaries of the hollow core. The vertical lines show the inner and outer boundaries of the hollow core.

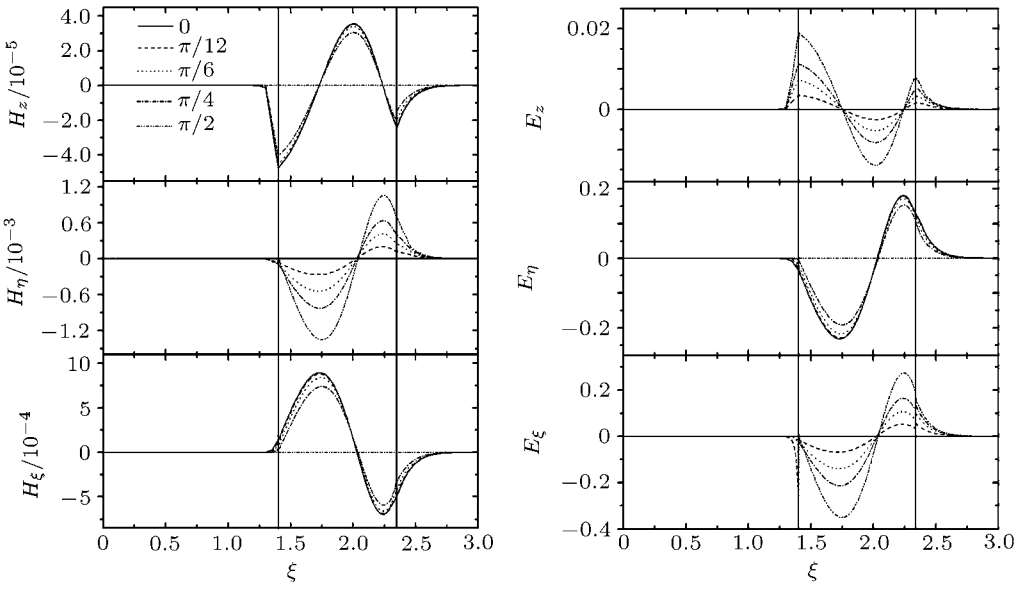



**Fig. 3.** The electric and magnetic field distributions for the ${}_{\rm e}{\rm HE}_{13}$ mode in the EDHF as functions of the radial position $\xi$. The parameters of the EDHF are the same as those in Fig. 2. The vertical lines show the inner and outer boundaries of the hollow core.

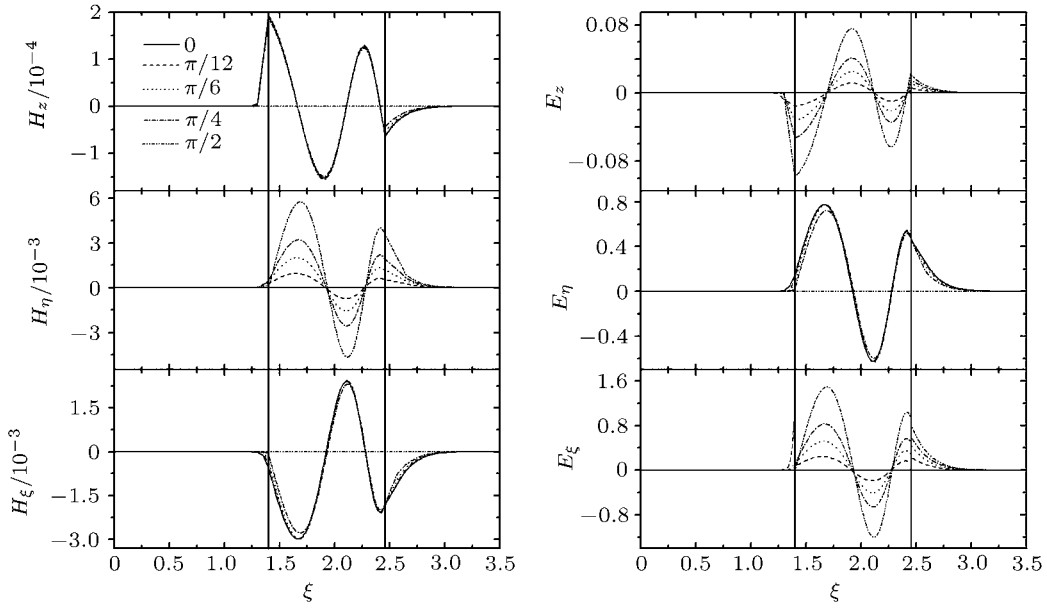



**Fig. 4.** The electric and magnetic field distributions for the $_{e}HE_{15}$ mode in the EDHF as functions of the radial position $\xi$. The parameters of the EDHF are the same as those in Fig. 2. The vertical lines show the inner and outer boundaries of the hollow core.

From Eqs. (7) and Figs. 2–4, we can see that for each mode, the magnitude of the distribution of $H_\xi$ is similar to that of $E_\eta$, while their phases are reversed. However, $H_\eta$ and $E_\xi$ have different magnitude curves, but the same phase. And we can further find that the longitudinal and transverse electromagnetic components $H_z$, $H_\xi$, and $E_\eta$ vanish at $\eta = \pi/2$ since these components are dependent on $\eta$ by involving the terms of circumferential modified and ordinary Mathieu functions $\mathrm{Qe}_m(\eta, q_i)$ and $\mathrm{Se}_m(\eta, q_i)$ and the differentials of $\mathrm{Qo}_m(\eta, q_i)$ and $\mathrm{So}_m(\eta, q_i)$ (here $m = 1$). In a similar manner, $E_z$, $E_\xi$, and $H_\eta$ vanish at $\eta = 0$ due to the $\mathrm{Qo}_m(\eta, q_i)$ and $\mathrm{So}_m(\eta, q_i)$ terms and the differentials of $\mathrm{Qe}_m(\eta, q_i)$ and $\mathrm{Se}_m(\eta, q_i)$ (here $m = 1$). Figures 2–4 also indicate that, in the longitudinal field distributions of the $_{e}HE_{11}$, $_{e}HE_{13}$, and $_{e}HE_{15}$ modes against the radial position $\xi$, the number of nodes equals $(n+1)/2$. While in their transverse field distributions, the number of nodes equals $(n-1)/2$. Here $n$ is the second subscript of the modes notation.

Through our numerical calculation, we also obtain that the distributions of the modes $_{e}HE_{11}$ and $_{e}HE_{12}$ versus the radial position $\xi$ have similar profiles, but opposite phases of $H_z$, $H_\xi$ and $E_\eta$. The same case happens to the modes $_{e}HE_{13}$ and $_{e}HE_{14}$, and so do the $_{e}HE_{15}$ and the $_{e}HE_{16}$ modes. Similarly, we can calculate and analyse the electromagnetic field distributions of other guided higher-order modes in EDHF and their propagating characteristics.

## 2.2. Intensity distribution of guided modes in EDHF

The intensity distribution of the guided modes in the EDHF can be calculated by using the longitudinal component of the time-averaged Poynting vector[32]

$$\begin{aligned} I(\xi) \propto \overline{S}_z &= \frac{1}{T}\int_0^T (\boldsymbol{E}\times\boldsymbol{H}^*)\cdot\boldsymbol{e}_z \mathrm{d}t \\ &= \frac{1}{2}(E_\xi H_\eta^* - E_\eta H_\xi^*) \\ &= \frac{1}{2}(\boldsymbol{E}_t \times \boldsymbol{H}_t^*)\cdot\boldsymbol{e}_z. \end{aligned} \tag{11}$$

From the numerical calculation, we obtain the normalised intensity distribution of the $_{e}HE_{11}$ mode at $\eta = 0$, i.e. in the horizontal direction, and figure 5 shows the result in the Cartesian coordinate system. We can see from Fig. 5 that the maximum intensity of evanescent-light wave near the inner wall surface of the EDHF is equal to several percents of the maximum intensity of the $_{e}HE_{11}$ mode in the core of the fibre, which is of very benefit to guide cold atoms or molecules in the EDHF by using the blue-detuned evanescent-light wave of the $_{e}HE_{11}$ mode.

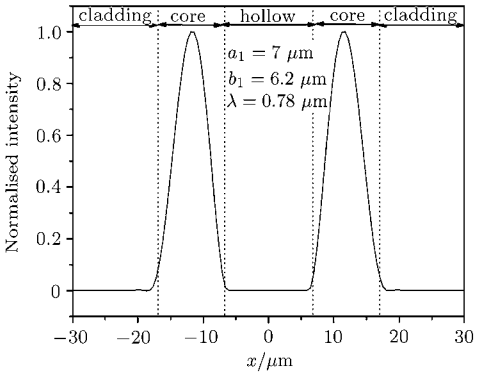



**Fig. 5.** Normalised intensity distribution of the $_{e}HE_{11}$ mode in the EDHF as a function of the position $x$ at ($a_1 = 7$ $\mu$m, $b_1 = 6.2$ $\mu$m, $n_0 = 1$, $n_1 = 1.4530$, $n_2 = 1.4502$, $e = 0.46$, $\lambda = 0.78$ $\mu$m). The vertical dashed lines show the two boundaries of EDHF.

We assume that the coupling and propagating loss of the $_{e}HE_{11}$ mode can be neglected as the length of the EDHF is very short (e.g. from a few cm to several tens of cm), and the incident beam with an input power $P_{in}$ is coupled into the core region of the EDHF. Hence the propagating power $P$ ($= P_{in}$) of the $_{e}HE_{11}$ mode in the EDHF can be written as

$$P = P_{in} = \int_s I(\xi)\mathrm{d}s = \int_0^{2\pi}\int_0^{\xi_3} I(\xi) \times h^2(\cosh^2\xi - \cos^2\eta)\mathrm{d}\xi\mathrm{d}\eta. \quad (12)$$

Using Eq. (12) and the relations between $A$, $B$, $C$, $D$, $A'$, $B'$, $C'$, and $D'$, we obtain the absolute intensity distribution of the $_{e}HE_{11}$ mode. When the input power is 0.5 W, the two-dimensional (2D) transverse intensity distribution of the $_{e}HE_{11}$ mode in the Cartesian coordinate system for $e = 0.46$ and $\lambda = 0.78$ $\mu$m is shown in Fig. 6(a), while figure 6(b) presents the 2D transverse intensity distribution of the $_{e}HE_{12}$ mode.

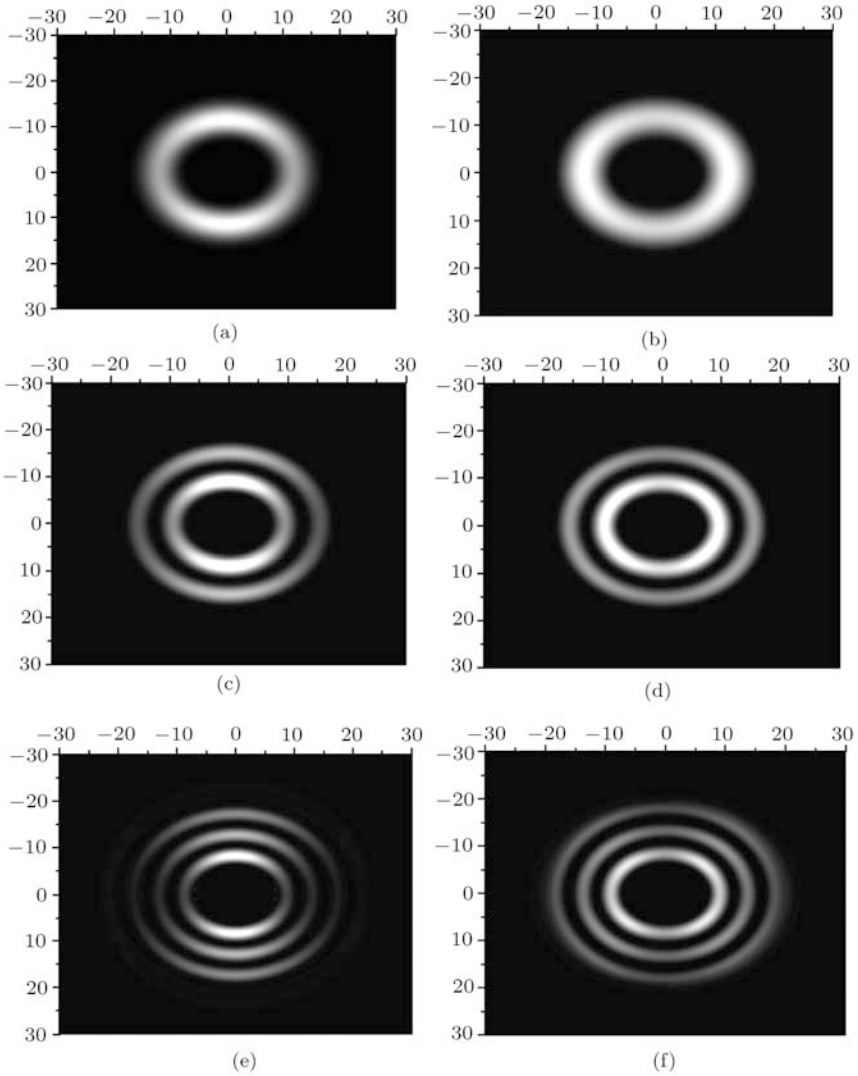



**Fig. 6.** The transverse intensity profile of (a) the $_{e}HE_{11}$ and (b) the $_{e}HE_{12}$ mode for $e = 0.46$ and $\lambda = 0.78$ $\mu$m; (c)–(f) show the profiles of the $_{e}HE_{13}$, $_{e}HE_{14}$, $_{e}HE_{15}$ and $_{e}HE_{16}$ modes respectively. Bright area indicates, the relative higher intensity, and the physical dimensions of the images are 30 $\mu$m×30 $\mu$m.

Using the same approach, we also can present the transverse intensity distributions of some other elliptical hollow modes, such as the ${}_{e}HE_{13}$, ${}_{e}HE_{14}$, ${}_{e}HE_{15}$ and ${}_{e}HE_{16}$ modes, which are respectively shown in Figs. 6(c) to 6(f). In Fig. 6, the bright area indicates higher intensity, and the maximum intensity can reach $10^9$ W/m$^2$.

By numerical calculation, we find that the transverse intensity distribution of the odd mode is similar to that of the corresponding even one. For both the even and odd modes, the maximum intensity along the ellipse long axis is different from that along the short axis, and the difference of the odd modes is larger than that of the corresponding even ones. From Fig. 6, we can find that (i) the maximum intensity of the ${}_{e}HE_{11}$, ${}_{e}HE_{13}$ and ${}_{e}HE_{15}$ modes (the second subscript $n$ is odd) in the transverse cross section is located at the ellipse short axis, while for the ${}_{e}HE_{12}$, ${}_{e}HE_{14}$ and ${}_{e}HE_{16}$ modes (the second subscript $n$ is even), the maximum intensity in the transverse cross section is located at the ellipse long axis, that is, they are perpendicular to each other. (ii) The Poynting vectors have the same propagation direction on the two sides of the boundary $\xi_0$, and so do they on the two sides of the boundary $\xi_1$, which is quite different from the case of an elliptic metallic waveguides.[26] (iii) The ${}_{e}HE_{11}$ and ${}_{o}HE_{11}$ modes, including their high-order modes, have a closed hollow intensity profile and some important applications in ultracold atomic physics and atom optics, cold molecular physics and molecule optics, etc., which will be discussed in the next section.

## 2.3. Polarisation states of single mode and its orbital angular momentum

It is well known from Maxwell's theory that the electromagnetic field carries both energy and momentum. The interaction of the electromagnetic field with matter involves not only the exchange of energy, but also the exchange of momentum, which has a linear or angular component. And the angular component has two parts: a spin one associated with polarization and an orbital one associated with spatial distribution. In this subsection, the polarization states of some hollow hybrid modes in the EDHF will be discussed in some detail. This will be helpful to the study of the dynamical properties of the light fields.

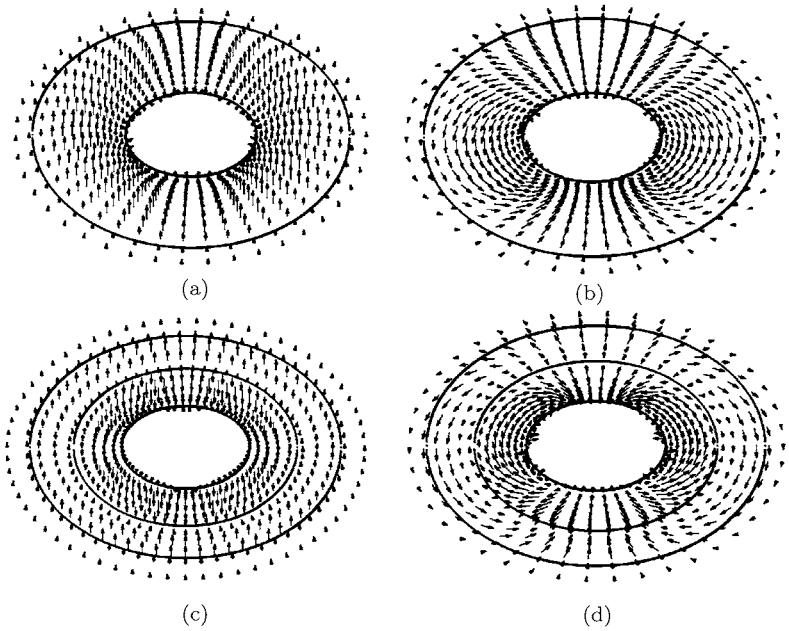



**Fig. 7.** Vector diagram of the transverse component of the electric field in the EDHF. Frames (a)–(d) are for the ${}_{e}HE_{11}$, ${}_{e}HE_{12}$, ${}_{e}HE_{13}$, ${}_{e}HE_{14}$ modes respectively. The two ellipses in (a) and (b) are the inner and outer boundaries of the hollow core. In (c) and (d), there is another ellipse between the two mentioned above, which indicates the lowest intensity of the light field.

Vector diagrams of the transverse components of the electric field for the even modes in the EDHF are shown in Fig. 7. Frames 7(a)–7(d) are respectively for the ${}_{e}HE_{11}$, ${}_{e}HE_{12}$, ${}_{e}HE_{13}$, ${}_{e}HE_{14}$ modes. And figures 8(a)–8(d) show the vector diagrams of the corresponding odd modes. The two ellipses in Figs. 7(a) and 7(b)

and Figs. 8(a) and 8(b) are the inner and outer boundaries of the hollow core. In each frame of Figs. 7(c) and 7(d) and 8(c) and 8(d), there is another ellipse between the two ellipses, which indicates the lowest intensity of the light field. The length and direction of the arrows in these plots denote the magnitude and orientation of the transverse vector electric field at different places. In the transverse $xoy$ plane, the orientation of the transverse vector electric fields can be obtained from

$$\frac{\mathrm{d}y}{\mathrm{d}x} = \frac{E_y}{E_x} = \frac{\cosh\xi \sin\eta E_\xi + \sinh\xi \cos\eta E_\eta}{\sinh\xi \cos\eta E_\xi - \cosh\xi \sin\eta E_\eta}. \tag{13}$$

Figures 7 and 8 show that the $\boldsymbol{E}$-field distributions of the odd modes in the cross section of the EDHF are the same as those of the even modes by rotating an angle of $\pi/2$, meanwhile the long axes of boundary ellipses are in perpendicular directions. For single propagation mode in optical fibres, the field at each point has a fixed orientation, and its magnitude varies in time in a given $z$ plane.

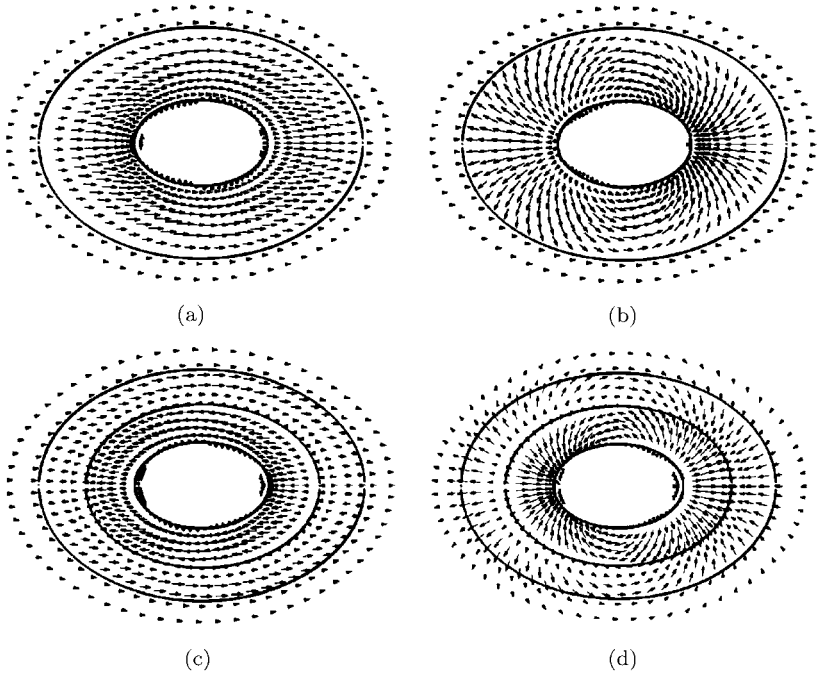



**Fig. 8.** Vector diagrams of the transverse component of the electric field for the ${}_{\mathrm{o}}\mathrm{HE}_{11}$, ${}_{\mathrm{o}}\mathrm{HE}_{12}$, ${}_{\mathrm{o}}\mathrm{HE}_{13}$, ${}_{\mathrm{o}}\mathrm{HE}_{14}$ modes are presented in frames (a)–(d) respectively. The two ellipses in (a) and (b) are the inner and outer boundaries of the hollow core. And the ellipse between the two stated above in (c) and (d) indicates the lowest intensity of the light field.

The OAM per photon in a light beam in the propagating direction, $\delta L_z$, can be calculated numerically by[33]

$$\begin{aligned}\delta L_z &= \frac{\iint \delta l_z(x,y) w(x,y) \mathrm{d}x\mathrm{d}y}{\iint w(x,y)\mathrm{d}x\mathrm{d}y} \\ &= \frac{\hbar\omega \iint j_z(x,y)\mathrm{d}x\mathrm{d}y}{\iint w(x,y)\mathrm{d}x\mathrm{d}y}.\end{aligned} \tag{14}$$

This shows that the OAM per photon in the beam, $\delta L_z$, can be written as the integral over the local OAM per photon, $\delta l_z$, weighted by the normalized energy density $w(x,y)$. Therefore, the OAM per photon can be calculated easily from the value of $w(x,y)$ for a finite number of points on a beam cross section. In the second equality of Eq. (14), $j_z(x,y)$ is the orbital angular momentum density, which can be written as[34]

$$j_z(x,y) = (\boldsymbol{r} \times \varepsilon \langle \boldsymbol{E} \times \boldsymbol{B} \rangle)_z = \varepsilon\mu_0 \boldsymbol{r} \times \langle \boldsymbol{E} \times \boldsymbol{H} \rangle_\phi, \tag{15}$$

where $\phi$ indicates the azimuthal component of time-averaged Poynting vector in the $xoy$ plane, and $w(x,y)$ can be given by

$$w(x,y) = |c\varepsilon\mu_0 \langle \boldsymbol{E} \times \boldsymbol{H} \rangle_z|. \tag{16}$$

It is easy to deduce from Eqs. (5)–(7) that the transverse Poynting vector of a single HE (EH) mode in the EDHF is exactly pure imaginary, which leads the time-averaged Poynting vector in the $xoy$ plane to zero. Hence, according to Eq. (14), the OAM per photon of single HE (EH) mode in the EDHF must be zero.

## 2.4. Dual-mode transmission in the EDHF

As is all known, the EDHF can not only transmit single mode, but also transmit dual-mode or multiple modes by adjusting the exciting conditions. In this section, we will briefly discuss dual-mode transmission in the EDHF, and the ${}_{\rm e}{\rm HE}_{11}$ mode and ${}_{\rm o}{\rm HE}_{11}$ mode are supposed to be selectively excited. The electric and magnetic fields can be given by

$$\begin{cases} E_z = r_{\rm e} E_{z{\rm e}} \exp\left(-{\rm i}\,\beta_{\rm e} z\right) + r_{\rm o} E_{z{\rm o}} \exp\left(-{\rm i}\,\beta_{\rm o} z\right), \\ E_\eta = -{\rm i}\, r_{\rm e} E_{\eta{\rm e}} \exp\left(-{\rm i}\,\beta_{\rm e} z\right) - {\rm i}\, r_{\rm o} E_{\eta{\rm o}} \exp\left(-{\rm i}\,\beta_{\rm o} z\right), \\ E_\xi = -{\rm i}\, r_{\rm e} E_{\xi{\rm e}} \exp\left(-{\rm i}\,\beta_{\rm e} z\right) - {\rm i}\, r_{\rm o} E_{\xi{\rm o}} \exp\left(-{\rm i}\,\beta_{\rm o} z\right), \\ H_z = r_{\rm e} H_{z{\rm e}} \exp\left(-{\rm i}\,\beta_{\rm e} z\right) + r_{\rm o} H_{z{\rm o}} \exp\left(-{\rm i}\,\beta_{\rm o} z\right), \\ H_\eta = -{\rm i}\, r_{\rm e} H_{\eta{\rm e}} \exp\left(-{\rm i}\,\beta_{\rm e} z\right) - {\rm i}\, r_{\rm o} H_{\eta{\rm o}} \exp\left(-{\rm i}\,\beta_{\rm o} z\right), \\ H_\xi = -{\rm i}\, r_{\rm e} H_{\xi{\rm e}} \exp\left(-{\rm i}\,\beta_{\rm e} z\right) - {\rm i}\, r_{\rm o} H_{\xi{\rm o}} \exp\left(-{\rm i}\,\beta_{\rm o} z\right). \end{cases} \tag{17}$$

Here $r_{\rm e}$ and $r_{\rm o}$ are parameters determined by the coupling efficiency of the ${}_{\rm e}{\rm HE}_{11}$ mode and ${}_{\rm o}{\rm HE}_{11}$ mode, and $\beta_{\rm e}$ and $\beta_{\rm o}$ are propagation constants of the two modes, respectively. $E_{z{\rm e}}$, $E_{\eta{\rm e}}$, $E_{\xi{\rm e}}$, $H_{z{\rm e}}$, $H_{\eta{\rm e}}$, and $H_{\xi{\rm e}}$ are magnitudes of the electric and magnetic fields of even modes, and $E_{z{\rm o}}$, $E_{\eta{\rm o}}$, $E_{\xi{\rm o}}$, $H_{z{\rm o}}$, $H_{\eta{\rm o}}$, and $H_{\xi{\rm o}}$ are those of odd modes, $z$ is the propagation distance and the time harmonic factor $\exp({\rm i}\,\omega t)$ is omitted.

We suppose $r_{\rm e} = r_{\rm o}$ here, the ${}_{\rm e}{\rm HE}_{11}$ mode and the ${}_{\rm o}{\rm HE}_{11}$ mode have similar intensity profiles [as shown in Fig. 6(a)], so that the dual-mode also has an elliptic hollow intensity distribution. And the vector diagram of the transverse component of the electric field for the dual-mode in the EDHF can be obtained from Eq. (13), which is shown in Fig. 9. The two ellipses are also the inner and outer boundaries of the hollow core. As to the dual-mode, the phase difference of the synthetic electric field components will be changed with the propagation distance $z$, and the orientation of the electric fields in the transverse $xoy$ plane will be changed as $z$ varies.

Moreover, as the phase difference of the synthetic field components changes with the propagation distance $z$, the OAM per photon of dual-mode in the EDHF is not necessarily equal to zero (Fig. 10). By using Eq. (15), the calculation of the time-averaged orbital angular momentum density $j_z(x, y)$ yields

$$\begin{aligned} j_z(x,y) = {} & h r_{\rm e} r_{\rm o} \sin[(\beta_{\rm e} - \beta_{\rm o})\, z][(E_{\eta{\rm o}} H_{z{\rm e}} - E_{\eta{\rm e}} H_{z{\rm o}} + E_{z{\rm o}} H_{\eta{\rm e}} - E_{z{\rm e}} H_{\eta{\rm o}}) \cos\eta \sin\eta \\ & + (E_{\xi{\rm e}} H_{z{\rm o}} - E_{\xi{\rm o}} H_{z{\rm e}} + E_{z{\rm e}} H_{\xi{\rm o}} - E_{z{\rm o}} H_{\xi{\rm e}}) \cosh\xi \sinh\xi] \,/\left(\sinh^2\xi + \sin^2\eta\right), \end{aligned} \tag{18}$$

and from Eq. (16) the energy density $w(x, y)$ is given by

$$\begin{aligned} w(x,y) = {} & c\varepsilon\mu_0[(E_{\xi{\rm e}} H_{\eta{\rm e}} - E_{\eta{\rm e}} H_{\xi{\rm e}})\, r_{\rm e}^2 + (E_{\xi{\rm o}} H_{\eta{\rm o}} - E_{\eta{\rm o}} H_{\xi{\rm o}})\, r_{\rm o}^2 \\ & + (E_{\xi{\rm o}} H_{\eta{\rm e}} + E_{\xi{\rm e}} H_{\eta{\rm o}} - E_{\eta{\rm o}} H_{\xi{\rm e}} - E_{\eta{\rm e}} H_{\xi{\rm o}})\, r_{\rm e} r_{\rm o} \cos\left((\beta_{\rm e} - \beta_{\rm o})\, z\right)]. \end{aligned} \tag{19}$$

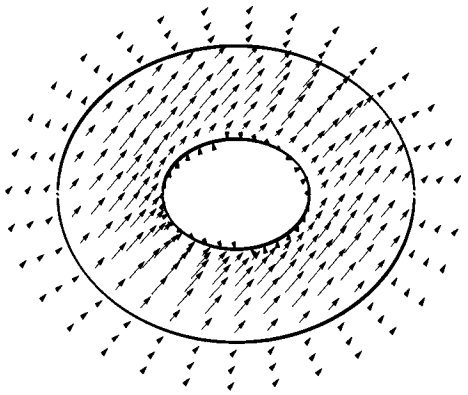


**Fig. 9.** Vector diagram of the transverse component of the electric field for the dual-mode in the EDHF. The two ellipses are also the inner and outer boundaries of the hollow core.

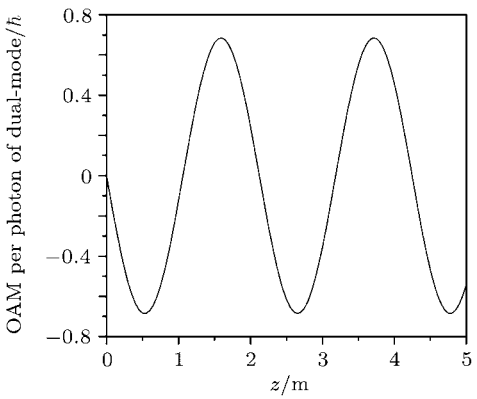



**Fig. 10.** OAM per photon of the dual-mode versus propagation distance $z$. Here $r_{\rm e} = r_{\rm o}$.

Then we can obtain the OAM per photon of the dual-mode in the EDHF by numerical integration. Figure 10 shows the OAM per photon of the dual-mode versus propagation distance $z$, which has an obvious sinusoidal oscillation that varies from $-0.68$ to $0.68\ \hbar$.

## 3. Potential applications

We have known that some of the guided elliptic modes (such as the ${}_{\rm e}{\rm HE}_{11}$ and ${}_{\rm o}{\rm HE}_{11}$ ones) in the EDHF are hollow ones. If the elliptic hollow evanescent-light waves in the hollow region are blue-detuned, due to ac Stark effect, then when a cold atom is moved and guided in a hollow evanescent-wave mode of the EDHF, the blue-detuned hollow evanescent-light wave will generate a repulsive optical potential for the guided cold atom, and push it to the central dark region of the field, so the evanescent-wave guiding of cold atoms in the EDHF is realised.

For a two-level atom, the optical potential $U(x)$ for cold atoms is given by[32]

$$U(x) = \frac{\hbar}{2}\delta \ln\left[1 + \frac{I(x)/I_s}{1 + 4(\delta/\Gamma)^2}\right], \tag{20}$$

where $\delta$ is the detuning of the laser frequency from the atomic resonance frequency, $I_{\rm s}$ and $\Gamma$ are the saturation intensity and the natural line width of the transition, respectively. For $^{85}$Rb $D_2$ line, $I_{\rm s} = 1.6\ {\rm mW/cm^2}$, and $\Gamma = 2\pi \times 6.0$ MHz. $I(x)$ is the intensity distribution of the elliptic hollow modes in the EDHF. Assuming that the input laser power is 0.5 W, the laser wavelength is near 0.78 $\mu$m, and the ${}_{\rm e}{\rm HE}_{11}$ mode is excited in the EDHF, we can calculate the efficient optical potential $U(x)$ of the ${}_{\rm e}{\rm HE}_{11}$ mode in the horizontal direction for $^{85}$Rb atoms, as shown in Fig. 11. We can see from Fig. 11(a) that with the increase of the laser detuning from 0.5 to 3 GHz, the optical potential will be increased from $\sim 0.9$ to $\sim 3$ K, and then it will be decreased as the laser detuning increases to 100 GHz. Figure 11(b) shows the optical potential of the evanescent-light wave in the hollow region. It can reach several tens of mK, which is deep enough to guide cold atoms from a standard $^{85}$Rb atomic MOT with a temperature of $\sim 120\ \mu$K, and also is of very benefit to reduce spontaneous-emitting rate of $^{85}$Rb atom in the hollow evanescent-light wave due to a larger blue-detuning.

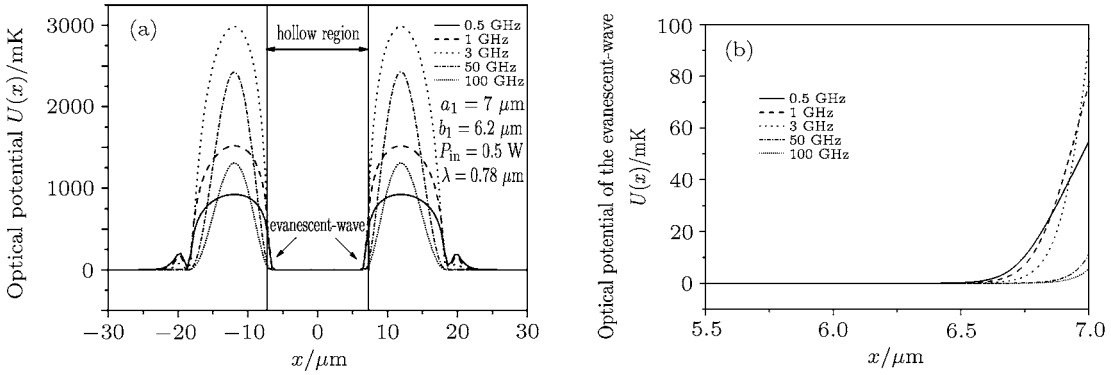



**Fig. 11.** (a) The optical potential $U(x)$ of the ${}_{\rm e}{\rm HE}_{11}$ mode in the EDHF for $^{85}$Rb atoms versus the horizontal position $x$ at $a_1 = 7\ \mu$m, $b_1 = 6.2\ \mu$m, $n_0 = 1$, $n_1 = 1.4530$, $n_2 = 1.4502$, $e = 0.46$, $\lambda = 0.78\ \mu$m, $P_{\rm in} = 0.5$ W. The vertical lines at $x = \pm 7\ \mu$m indicate the inner boundary of the hollow core. (b) The detail of the optical potential of the evanescent-light wave.

Since the EDHF is micron-sized and the efficient interaction region of the evanescent-light waves is less than a laser wavelength away from the inner surface of the hollow core, we should consider the position-dependent van der Waals attractive potential from an inner surface of the elliptic hollow core. It can result from the cavity QED effect, and for a cold atom in the ground state, the position-dependent van der Waals potential is of the following form[35]

$$U_{\rm CP}(x) = -\sum_{\rm e} \frac{(2J_{\rm e}+1)h\Gamma_{\rm eg}\lambda_{\rm eg}^3}{256\pi^2 a_1^3} \int_0^\infty \rho^2 {\rm d}\rho \frac{\cosh(\pi\rho x/a_1)}{\sinh(\pi\rho)} \arctan\left(\frac{\rho\lambda_{\rm eg}}{4a_1}\right) \frac{n_1^2 - 1}{n_1^2 + 1}, \tag{21}$$

where $x$ denotes the position in the horizontal direction, the summation runs over all excited states, $\lambda_{\rm eg}$ is the wavelength of the $|{\rm e}\rangle \to |{\rm g}\rangle$ transition, $\Gamma_{\rm eg}$ is the natural line width, and $\rho$ is a dummy variable. Then the total guiding potential for cold $^{85}$Rb atoms, reduced by the cavity QED effect, can be given[35]

$$U_{\rm TP}(x) = U_{\rm OP}(x) + \eta_{\rm Geo} U_{\rm CP}(x), \qquad (22)$$

where $\eta_{\rm Geo}$ is a geometric factor for the elliptic cylinder cavity, which varies between 1 and 10.[36] We assume $\delta = 1$ GHz and $\eta_{\rm Geo} = 5$, and obtain the total potential barrier in terms of temperature, as shown in Fig. 12. We only plot the main region of the total guiding potential $U(x)$. It is clear from Fig. 12 that when $\delta = 1$ GHz and $P = 0.5$ W, the maximum potential barrier is greater than 50 mK, which is high enough to guide cold $^{85}$Rb atoms from a standard MOT with a temperature of $\sim 120$ $\mu$K.

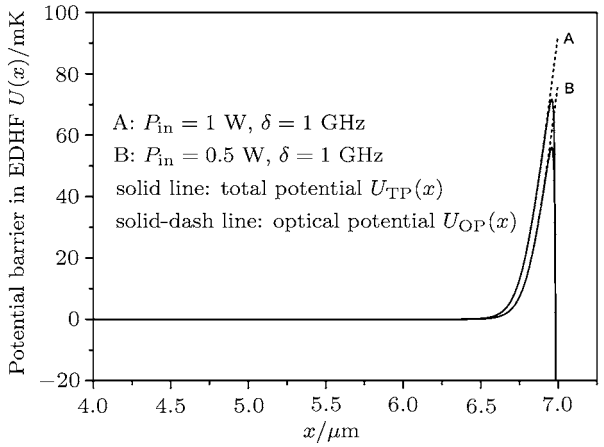



**Fig. 12.** The total guiding potential $U(x)$ of the $_{\rm e}{\rm HE}_{11}$ mode in the EDHF for $^{85}$Rb atoms versus the horizontal position $x$ for $a_1 = 7$ $\mu$m, $b_1 = 6.2$ $\mu$m, $n_0 = 1$, $n_1 = 1.4530$, $n_2 = 1.4502$, $e = 0.46$, $\lambda = 0.78$ $\mu$m, $P_{\rm in} = 1$ W or 0.5 W, including the optical potential of the $_{\rm e}{\rm HE}_{11}$ mode in the EDHF and the cavity attractive potential from an inner surface of the elliptic hollow core. In the horizontal position of 0–4 $\mu$m, the total guiding potential $U(x)$ is small enough to approach zero.

On the other hand, from Subsections 2.2 and 2.4, we can see that if let an elliptic hollow mode be diffracted output at the outlet of the EDHF, a high-order elliptic hollow beam with a divergent angle will be generated, that is, a short EDHF with a few micron in hollow size can be used to generate some high-order elliptic hollow beams with a fractional angular momentum, which is similar to the generation of dark hollow beam by a small cylindrical hollow fibre[4] and can be used to study the transfer of the angular momentum from the light field to cold atoms, even to study matter-wave vortexes (fraction quantum Hall effect) with a fractional angular momentum in the guided BEC atoms, etc.

# 4. Conclusions

In this paper, we have investigated the electromagnetic field distributions, Poynting vector distribution, polarization states and orbital angular momentum of $_{\rm e}{\rm HE}_{11}$ mode, the high-order $_{\rm e}{\rm HE}_{12}$, $_{\rm e}{\rm HE}_{13}$, and $_{\rm e}{\rm HE}_{15}$ modes; and also those of the corresponding odd modes in a micron-sized EDHF, and briefly analyse the dual-mode transmission in the EDHF. Our study shows that i) the $\boldsymbol{E}$-field distributions of the odd modes in the cross section of the EDHF are the same as those of the even modes by rotating an angle of $\pi/2$, but the boundary ellipses are different; ii) the per-photon OAM of single HE (EH) mode is exactly equal to zero, while that of dual-mode in the EDHF is fractional in $\hbar$, and has a sinusoidal oscillation as $z$ varies.

Moreover, we have briefly discussed some potential applications of the above elliptic hollow modes in atom and molecule optics, and found that the blue-detuned hollow evanescent-wave modes can be used to guide cold atoms in the hollow region of the EDHF, and this scheme can also be used to generate various high-order elliptic hollow beams with fractional angular momenta. If monochromatic sources of ultracold atoms are gained, single-mode propagation in the EDHF can maintain coherence of the matter-waves, while multimode propagation does not.[37,38] Because the orbital angular momentum per photon of the elliptical dual-mode in the EDHF is usually fractional in $\hbar$, the interaction of the output light field with cold atoms, molecules or other microparticles should be more worthy of research. The electromagnetic vortices formed by an elliptic optical field can be used as optical waveguides and atom traps,[39] which can be also used to study the transfer of angular momentum from the light field to atoms, molecules or other microparticles.[40−42] In addition, researches on the interaction of its angular momentum with the internal states of molecular systems[43] or on the creation of nucleation vortices in atomic or molecular Bose–Einstein condensates[44−46] should be very interesting.

# Acknowledgements

The authors would like to acknowledge Alhargan F. A. and Xiong T. X. for their helpful discussions.

# References


[1] Accatino L, Bertin G and Mongiardo M 1997 *IEEE Trans. Microwave Theory Tech.* **45** 2393

[2] Rengarajan S R and Lewis J E 1980 *IEEE Trans. Microwave Theory Tech.* **28** 1085

[3] Choi S and Oh K 2003 *Opt. Commun.* **221** 307

[4] Yin J P, Noh H R, Lee K, Kim K H, Wang Y Z and Jhe W 1997 *Opt. Commun.* **138** 287

[5] Yin J P, Gao W J, Wang H F, Long Q and Wang Y Z 2002 *Chin. Phys.* **11** 1157

[6] Renn M J, Montgomery D, Vdovin O, Anderson D Z, Wieman C E and Cornell E A 1995 *Phys. Rev. Lett.* **75** 3253

[7] Renn M J, Donley E A, Cornell E A, Wieman C E and Anderson D Z 1996 *Phys. Rev.* A **53** R648

[8] Ito H, Nakata T, Sakaki K, Ohtsu M, Lee K I and Jhe W 1996 *Phys. Rev. Lett.* **76** 4500

[9] Wang Z L, Dai M, Yin J P and Wang Z L 2005 *Opt. Express* **13** 8406

[10] Ni Y, Liu N C and Yin J P 2003 *J. Opt.* B: *Quantum Semiclass. Opt.* **5** 300

[11] Yin J P, Gao W J and Zhu Y F 2003 *Prog. Opt.* **45** 119

[12] Yeh C 1962 *J. Appl. Phys.* **33** 3235

[13] Chu L J 1938 *J. Appl. Phys.* **9** 583

[14] Kretzsch J G 1970 *IEEE Trans. Microwave Theory Tech.* **MT18** 547

[15] Kretzsch J G 1972 *IEEE Trans. Microwave Theory Tech.* **MT20** 280

[16] Falciase G, Someda C G and Valdoni F 1973 *IEEE Trans. Microwave Theory Tech.* **MT21** 154

[17] Rengarajan S R and Lewis J E 1979 *Electron. Lett.* **15** 637

[18] Goldberg D A, Laslett L J and Rimmer R A 1990 *IEEE Trans. Microwave Theory Tech.* **38** 1603

[19] Valenzuela G R 1960 *IRE Trans. Microwave Theory Tech.* **8** 431

[20] Rengarajan S R and Lewis J E 1981 *Radio Sci.* **16** 541

[21] Shu C 2000 *IEEE Trans. Microwave Theory Tech.* **48** 319

[22] Zhang S J and Shen Y C 1995 *IEEE Trans. Microwave Theory Tech.* **43** 227

[23] Schneider M and Marquardt J 1999 *IEEE Trans. Microwave Theory Tech.* **47** 513

[24] Young D L, Hu S P, Chen C W, Fan C M and Murugesan K 2005 *Microwave Opt. Tech. Lett.* **44** 552

[25] Xiong T X and Yang R G 2004 *J. Southwest Jiaotong Univ.* **12** 130

[26] Halterman K, Feng S and Overfelt P L 2007 *Phys. Rev.* A **76** 013834

[27] Gomez-Castellanos I and Rodriguez-Dagnino R M 2007 *Opt. Eng.* **46** 45003

[28] Nair V M, Sarkar S and Khijwania S K 2008 *IEEE Photonics Tech. Lett.* **20** 1381

[29] Abramowitz M and Stegun I 1964 *Handbook of Mathematical Functions* (New York: Dover) pp. 721–750

[30] Morse P and Feshbach H 1953 *Methods of Theoretical Physics* (New York: McGraw-Hill)

[31] Alhargan F A 2000 *ACM Trans. Math. Softw.* **26** 390

[32] Ito H, Sakaki K, Nakata T, Jhe W and Ohtsu M 1995 *Opt. Commun.* **115** 57

[33] Chávez-Cerda S, Padgett M J, Allison I, New G H C, Gutiérrez-Vega J C, O'Neil A T, MacVicar I and Courtial J 2002 *J. Opt.* B: *Quantum Semiclass. Opt.* **4** S52

[34] Allen L, Beijersbergen M W, Spreeuw R J C and Woerdman J P 1992 *Phys. Rev.* A **45** 8185

[35] Yin J P, Zhu Y F and Wang Y Z 1998 *Phys. Rev.* A **57** 1957

[36] Ito H, Sakaki K, Nakata T, Jhe W H and Ohtsu M 1995 *Ultramicroscopy* **61** 91

[37] Marksteiner S, Savage C M, Zoller P and Rolston S L 1994 *Phys. Rev.* A **50** 2680

[38] Duan Z L, Zhang W P, Li S Q, Zhou Z Y, Feng Y Y and Zhu R 2005 *Acta Phys. Sin.* **54** 5622 (in Chinese)

[39] Xu S H, Li Y M and Lou L R 2006 *Chin. Phys.* **15** 1391

[40] Gahagan K T and Swartzlander G A 1999 *J. Opt. Soc. Am.* B **16** 533

[41] Simpson N B, Dholakia K, Allen L and Padgett M J 1997 *Opt. Lett.* **22** 52

[42] Lopez-Mariscal C, Gutierrez-Vega J C, Milne G and Dholakia K 2006 *Opt. Express* **14** 4182

[43] Babiker M, Bennett C R, Andrews D L and Davila Romero L C 2002 *Phys. Rev. Lett.* **89** 143601

[44] Aftalion A and Blanc X 2008 *Ann. I. H. Poincaré-AN.* **25** 339

[45] Andersen M F, Ryu C, Clade P, Natarajan V, Vaziri A, Helmerson K and Phillips W D 2006 *Phys. Rev. Lett.* **97** 170406

[46] Wright K C, Leslie L S and Bigelow N P 2008 *Phys. Rev.* A **78** 041601